Hall effect in cuprates with an incommensurate collinear spin-density wave

M. Charlebois,[1] S. Verret,[1] A. Foley,[1] O. Simard,[1] D. Sénéchal,[1] and A.-M. S. Tremblay[1,2]
[1]*Département de Physique and Institut quantique, Université de Sherbrooke, Sherbrooke, QC, Canada*
[2]*Canadian Institute for Advanced Research, Toronto, Ontario, Canada*
(Received 29 August 2017; published 16 November 2017)

The presence of incommensurate spiral spin-density waves (SDW) has been proposed to explain the p (hole doping) to $1+p$ jump measured in the Hall number n_H at a doping p^*. Here we explore incommensurate *collinear* SDW as another possible explanation of this phenomenon, distinct from the incommensurate *spiral* SDW proposal. We examine the effect of different SDW strengths and wave vectors, and we find that the $n_H \sim p$ behavior is hardly reproduced at low doping. Furthermore, the calculated n_H and Fermi surfaces give characteristic features that should be observed; thus, the lack of these features in experiment suggests that the incommensurate collinear SDW is unlikely to be a good candidate to explain the $n_H \sim p$ observed in the pseudogap regime.

DOI: 10.1103/PhysRevB.96.205132

I. INTRODUCTION

Recently, a measurement of the Hall effect in $YbBa_2Cu_3O_y$ (YBCO) by Badoux *et al.* [1] provided some clues on the zero-temperature normal state that is found when a magnetic field prohibits superconductivity. A sharp jump in the effective carrier density from p (hole doping) to $1+p$ was observed around $p^* \sim 0.19$, the extrapolated zero-temperature value of the pseudogap line $T^*(p)$ [2]. It was suggested that this is an important clue to understand the pseudogap phenomenon.

Since then, an appreciable number of phenomenological theories were proposed to explain this behavior. Most of them reproduced the jump in the effective carrier number measured from the Hall effect n_H. The candidate theories can be separated in two groups: those based on a hypothetical long-range magnetic order and those based on Mott-like physics.

In the first group, a simple antiferromagnet [3] was shown sufficient to reproduce the p behavior at low doping. However, in experiments, antiferromagnetism does not extend above $p = 0.05$ [4] and, therefore, this scenario is unlikely. Spiral antiferromagnets, commensurate and incommensurate, were also studied [5]. In the incommensurate case (above $p = 0.05$), hole pockets twice as large as in the simple antiferromagnet were predicted. This would show up in quantum oscillations.

In the second group of theories, based on Mott physics, the resonating-valence-bond spin-liquid ansatz of Yang *et al.* (YRZ) [6], a phenomenological model of the pseudogap, was able to reproduce the jump in Hall carrier [3]. An implementation of the fractionalized Fermi liquid theory (FL*) was also able to reproduce this jump [7].

All of the above theories can be expressed as two-band effective models [8]. In other words, a strong-enough order, introduced as an effective mean field, opens a gap at half-filling, splitting a single band into two bands. This regime is associated with an effective carrier density p. If this mean field order is removed, one recovers the original single band with an effective carrier density of $1+p$. Each theory that reproduces the Hall jump [1] tunes this mean field as a function of doping to recover the two bands (p) at low doping and a single band ($1+p$) above p^*. The charge-density d-wave superconductivity SU(2) theory gave a different explanation of this same jump [9].

In this paper, we explore another possibility: the incommensurate collinear spin-density wave (SDW, see Fig. 1) [10]. By collinear, we mean a SDW that is a modulation of the amplitude of the spin order parameter by contrast with the spiral SDW, which is a rotation of the spin with constant amplitude [11,12]. It is not clear experimentally whether the SDW is spiral or collinear, as discussed in the context of $La_{2-x}Sr_xCuO_4$ (LSCO) measurements [10]. But we do know that for $p > 0.05$, there is an incommensurate SDW that survives at low temperature, either collinear or spiral. This has been found by neutron scattering in LSCO and YBCO [4,13,14].

Since calculations for the spiral SDW have already been done [5], we focus only on the long-range incommensurate collinear SDW. The tight-binding Hamiltonian along with the formalism used to evaluate the Hall number n_H is shown in Sec. II. In Sec. III, we present results following a very gradual approach: we compute n_H as a function of p, first without SDW, then with a commensurate SDW, and finally with incommensurate SDW. This progression reveals the effect of each modification and builds a general understanding that will be useful for our discussion (Sec. IV). In the end, we show how unlikely it is that the incommensurate collinear SDW explains the jump in Hall carrier. We conclude that if an order is associated with the pseudogap at $T = 0$, it is probably best represented by a two-band effective model.

II. MODEL

We use the following tight-binding Hamiltonian:

$$H = \sum_{\mathbf{k},\sigma} \xi_{\mathbf{k}} c^\dagger_{\mathbf{k},\sigma} c_{\mathbf{k},\sigma} + M \sum_{\mathbf{k},\sigma} \sigma (c^\dagger_{\mathbf{k},\sigma} c_{\mathbf{k}+\mathbf{Q},\sigma} + \text{H.c.}). \quad (1)$$

The first term is the kinetic energy, where the dispersion relation $\xi_{\mathbf{k}}$ is defined with first-, second-, and third-neighbor hopping energy t, t', and t'':

$$\begin{aligned}\xi_{\mathbf{k}} = &-2t(\cos(k_x) + \cos(k_y)) \\ &- 2t'(\cos(k_x + k_y) + \cos(k_x - k_y)) \\ &- 2t''(\cos(2k_x) + \cos(2k_y)) - \mu. \end{aligned} \quad (2)$$

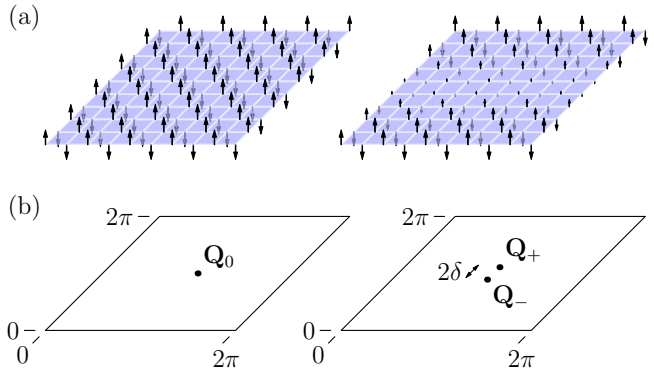

FIG. 1. (a) Local moment distributions for commensurate (π,π) collinear SDW (left) and incommensurate collinear SDW (right). The incommensurate SDW is the equivalent to a commensurate SDW modulated by $\cos(2\pi\delta\hat{\mathbf{y}})$. Here, $L = 9$ and $\delta = \frac{1}{18}$ (see Sec. II B for definitions). (b) $\mathbf{Q}$ in the reciprocal space for commensurate collinear SDW (left) and incommensurate collinear SDW (right).

The second term of Hamiltonian Eq. (1) is the SDW mean-field energy with amplitude M. $c^\dagger_{\mathbf{k},\sigma}$ and $c_{\mathbf{k},\sigma}$ are the creation and annihilation operators of momentum $\mathbf{k}$. $\mathbf{Q}$ is the wave vector of the SDW.[1] $\sigma = \pm 1$ is the spin index. We work in units where Planck's constant and lattice spacing are unity.

The commensurate (π,π) SDW is presented in Sec. II A and the incommensurate collinear SDW in Sec. II B. Both SDW are shown in Fig. 1. It is important to emphasize that we do not solve the truly incommensurate case but only rational approximations, namely commensurate SDW with shorter or longer periods, depending on the definition of $\mathbf{Q}$. This distinction between commensurate (π,π) SDW and incommensurate SDW is consistent with common usage in experiments.

A. Commensurate case

When the wave vector is

$$\mathbf{Q}_0 = (\pi,\pi), \tag{3}$$

the SDW is commensurate with period 2 in x and y directions; it corresponds exactly to the spin ordering of an Néel antiferromagnet. In that case, we can define the following two-orbital spinor:

$$\Psi^\dagger_{\mathbf{k},\sigma} = (c^\dagger_{\mathbf{k},\sigma}\, c^\dagger_{\mathbf{k}+\mathbf{Q}_0,\sigma}), \tag{4}$$

and matrix Hamiltonian

$$\hat{H}_{\mathbf{k},\sigma} = \begin{pmatrix} \xi_{\mathbf{k}} & \sigma M \\ \sigma M & \xi_{\mathbf{k}+\mathbf{Q}_0} \end{pmatrix}, \tag{5}$$

so that the original Hamiltonian Eq. (1) can be expressed as

$$H = \sum_{\substack{\mathbf{k}\in \mathrm{rBz} \\ \sigma}} \Psi^\dagger_{\mathbf{k},\sigma} \hat{H}_{\mathbf{k},\sigma} \Psi_{\mathbf{k},\sigma}. \tag{6}$$

[1]Only considering $\mathbf{Q}$ is sufficient to generate smaller gaps at the harmonics $2\mathbf{Q}$, $3\mathbf{Q}$, and so on, through the diagonalization of the Hamiltonian.

The sum is restricted to the reduced Brillouin zone (rBz) to avoid double counting. In the commensurate case, this rBz corresponds to the antiferromagnetic Brillouin zone. The eigenenergies $E_{\mathbf{k},n}$ (for band n) are simply obtained through diagonalization of the $H_{\mathbf{k},\sigma}$ matrix.

B. Incommensurate case

In cuprates, the SDW does not remain commensurate for every doping. Beyond a threshold, it becomes incommensurate. The single SDW vector $\mathbf{Q}_0$ then splits locally in two wave vectors:

$$\mathbf{Q}_\pm = 2\pi\left(\frac{1}{2},\frac{1}{2} \pm \delta\right), \tag{7}$$

as experimentally measured with neutron scattering on single crystals [4,14] (see Fig. 1). Higher order harmonics are negligible. Note that this order breaks C_4 rotational symmetry.

We can generalize the approach above in a straightforward way for incommensurate SDW by defining the spinor of dimension $2L$:

$$\Psi^\dagger_{\mathbf{k},\sigma} = (c^\dagger_{\mathbf{k},\sigma}, \ldots\, c^\dagger_{\mathbf{k}+m\mathbf{Q}_+,\sigma}\, \ldots), \tag{8}$$

where m ranges from 0 to $2L-1$. $2L$ is an even integer that defines the denominator of the fraction of the incommensurability:

$$\delta = \frac{q}{2L}, \tag{9}$$

with q an integer. With this spinor definition, the original Brillouin zone is then separated in $2L$ rBz. Hence, with $2L$ additions of the vector $\mathbf{Q}_+$, modulo a vector of the reciprocal lattice,[2] we cycle through every different rBz. Note that we need an even number of additions of $\mathbf{Q}_+$ to cycle through every different rBz. We could use $\mathbf{Q}_-$ and it would cover the exact same $2L$ rBz since $\mathbf{Q}_+ = -\mathbf{Q}_-$ modulo a vector of the reciprocal lattice.

The Hamiltonian matrix $\hat{H}_{\mathbf{k},\sigma}$ in this basis is of dimension $2L$ by $2L$. It has $\epsilon_{\mathbf{k}+m\mathbf{Q}_+}$ on the diagonal and zero on most of the off-diagonal elements. When the column index m and the row index m' are such that $m - m'$ modulo $2L$ is ± 1, the matrix element is the scalar σM. This matrix is almost, but not quite, tridiagonal due to the finite term at indices $(m,m') = (1,2L)$ and $(2L,1)$.

We name this representation where $\delta \neq 0$ "incommensurate SDW." However, in reality, it is commensurate with a long period. In other words, since δ is a fraction, the only order that can be represented by our model repeats every $2L$ sites in the y direction and every 2 sites in the x direction.

Note that with $\delta = 0$, we recover the commensurate model of the previous section.

C. Formula for the Hall conductivity

With $\hbar = 1$, the electron charge e and the normalization volume V, the Hall number n_H and resistivity R_H are [8,15]:

$$R_H = \frac{\sigma_{xy}}{\sigma_{xx}\sigma_{yy}} = \frac{V}{e n_H}, \tag{10}$$

[2]Of the original Brillouin zone.

where σ_{xx} is the longitudinal conductivity at zero temperature in the zero-frequency limit when interband transitions can be neglected:

$$\sigma_{xx} = \frac{e^2\pi}{V} \sum_{\substack{n \\ \mathbf{k}\in \mathrm{rBz}}} \left(\frac{\partial E_{\mathbf{k},n}}{\partial k_x}\right)^2 A^2_{\mathbf{k},n}(0), \tag{11}$$

and σ_{xy} is the transversal conductivity [3,5,8,15]:

$$\sigma_{xy} = \frac{e^3\pi^2}{3V} \sum_{\substack{n \\ \mathbf{k}\in \mathrm{rBz}}} \left[-2\frac{\partial E_{\mathbf{k},n}}{\partial k_x}\frac{\partial E_{\mathbf{k},n}}{\partial k_x}\frac{\partial^2 E_{\mathbf{k},n}}{\partial k_x \partial k_y} + \left(\frac{\partial E_{\mathbf{k},n}}{\partial k_x}\right)^2 \frac{\partial^2 E_{\mathbf{k},n}}{\partial k_y^2} + \left(\frac{\partial E_{\mathbf{k},n}}{\partial k_y}\right)^2 \frac{\partial^2 E_{\mathbf{k},n}}{\partial k_x^2} \right] A^3_{\mathbf{k},n}(0). \tag{12}$$

$E_{\mathbf{k},n}$ is the eigenenergy of band n. Here, the band index n includes the spin index σ. $A_{\mathbf{k},n}(\omega)$ is the spectral weight for band n:

$$A_{\mathbf{k},n}(\omega) \equiv -\frac{1}{\pi}\mathrm{Im}\left(\frac{1}{\omega + i\eta - E_{\mathbf{k},n}}\right). \tag{13}$$

The Lorentzian broadening η is necessary for the integral to converge and corresponds to constant lifetime $\tau = \frac{1}{2\eta}$. We choose $\eta = 0.05$. However, a different value with the same magnitude yields similar results [8].

The derivatives $\frac{\partial E_{\mathbf{k},n}}{\partial k_\alpha}$ are the Fermi velocities in the $\alpha = x, y$ direction and $\frac{\partial^2 E_{\mathbf{k},n}}{\partial k_\alpha \partial k_\beta}$ corresponds to the $\alpha\beta$ component of the inverse effective mass tensor. When the above formulas are used, it is important to use the derivatives of the eigenenergies $E_{\mathbf{k},n}$ and not of the bare band $\xi_{\mathbf{k}}$ to capture the correct behavior of the Hall effect [3,5,8,15]. For an arbitrary given $\mathbf{k}$ point, it is easy to compute the $\hat{H}_{\mathbf{k},\sigma}$ matrix and find its eigenenergies $E_{\mathbf{k},n}$. However, it is more complicated to obtain their derivatives for matrices larger than 2×2. Appendix A shows a systematic approach to calculate exactly these derivatives with a single diagonalization of the matrix $\hat{H}_{\mathbf{k},\sigma}$ at each $\mathbf{k}$ point by a generalization of the Hellmann-Feynman theorem [16,17].

III. RESULTS

In this section, we look at the Hall number n_H as a function of hole doping p relative to half-filling. We choose this convention to match the experimental data and theoretical studies in hole-doped cuprates [1,3,5,18]. With this convention, the p axis goes from a completely filled band at $p = -1$ to an empty band at $p = 1$, with $p = 0$ corresponding to half-filling. We will study in detail three cases to understand progressively the complications of the underlying physics and to familiarize ourselves with the general behavior of n_H versus p curves.

A. No SDW

Let us first look at the behavior of n_H as a function p for the bare band without any density wave ($M = 0$). In Fig. 2, we present the Hall conductivity for three different band parameters (t',t'') and their corresponding Fermi surface

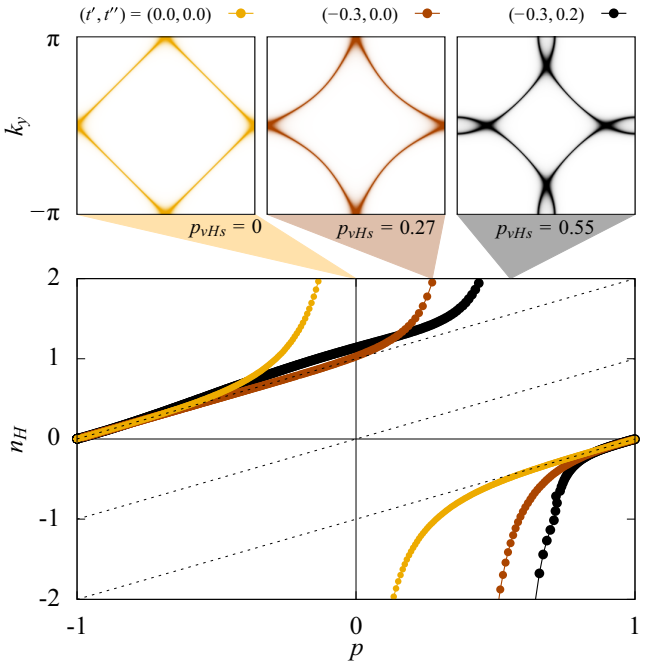

FIG. 2. (bottom) Hall conductivity n_H as a function hole doping p for three different band parameters. (top) Fermi surfaces ($\sum_n A_{\mathbf{k},n}(0)$) at p_{vHs} of each of the three band parameters. The color in the legend specifies which curve and Fermi surface correspond to which band parameter. Yellow corresponds to the particle-hole symmetric case and black corresponds to an approximation to the band parameters of YBCO as calculated from density functional theory without interactions [19,20]. Hence, brown corresponds to an intermediate case, to show the effect of neglecting t''. We define the reference $t = 1$, which corresponds to approximately 250 meV in YBCO. $p = 1$ corresponds to an empty band (no electron), and $p = -1$ corresponds a completely full band. The triangles below the Fermi surface graphs show the doping corresponding to each Fermi surface, hence to each van Hove singularity. We see on the brown curve that this doping is not equal to the doping where $R_H = 0$. The three dotted lines correspond to $p - 1$, p, and $p + 1$.

at the van Hove singularity (vHs). This figure allows us to understand three general facts.

First, for any band parameter, a filled band (at $p \sim -1$) always behaves like a free hole gas (n_H is the number of holes in the band) whereas an empty band (at $p \sim 1$) always behaves like a free electron gas (n_H is minus the number of electrons in the band). Hence, n_H changes signs between $p = -1$ and $p = 1$. It implies that at some doping p_0, the number of holelike carriers must be equal to the number of electronlike carriers, hence $R_H = 0$. When this happens, n_H diverges. $R_H = 0$ can happen for more than one doping, as we will see in the next sections. Changing the band structure $\xi_{\mathbf{k}}$ only changes the value of the doping p_0, but the general behavior found in Fig. 2 is the same.

Second, although the doping p_0 is always close to the doping of the van Hove singularity p_{vHs}, they are not always the same. The chemical potential corresponding to p_{vHs} can be determined exactly by analytical calculation (Appendix B). Both dopings p_0 and p_{vHs} are equal only for $(t',t'') = (0,0)$. For $(t',t'') = (-0.3,0.0)$, there is a clear offset between p_0

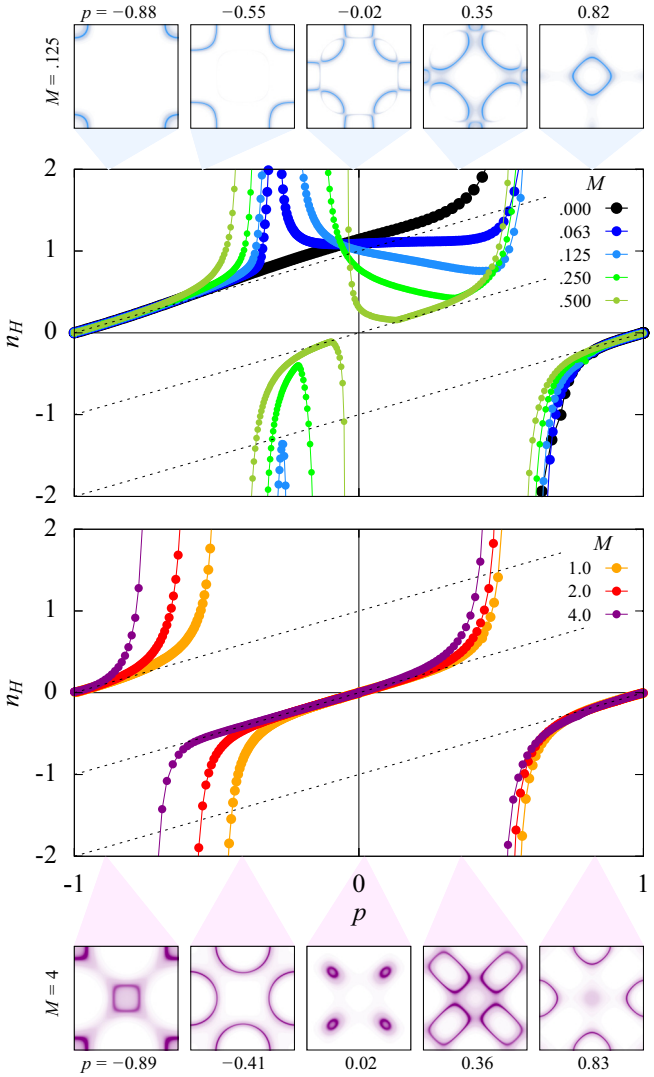

FIG. 3. The middle two panels show the Hall number n_H as a function of the hole doping p relative to half-filling for different SDW amplitudes M ($\delta = 0$). The outer panels show the Fermi surface for five different dopings for $M = 0.125$ (top blue Fermi surfaces) and for $M = 4.0$ (bottom purple Fermi surfaces). The triangles below and above the Fermi surface graphs show the doping corresponding to each Fermi surface. The three dotted lines correspond to $p - 1$, p, and $p + 1$. Here, $t' = -0.3$, $t'' = 0.2$.

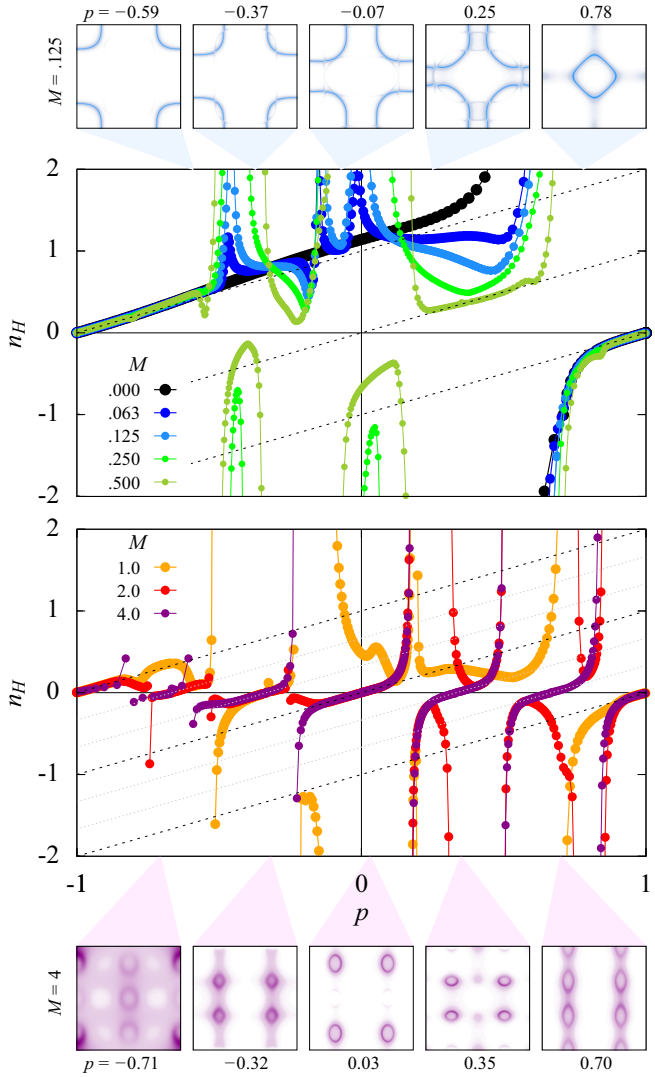

FIG. 4. Same as Fig. 3 but with $\delta = 1/6$.

and p_{vHs}. However, the two dopings are always close because there are rapid changes in the Fermi surface near the van Hove singularity, causing rapid changes in the nature of charge carriers.

Third, t'' has an impact as important as t' on the values of p_0 and p_{vHs}, so we must not neglect it.

B. Commensurate SDW ($\delta = 0$)

Let us now look at the antiferromagnetic case. In Fig. 3, we show the Hall number n_H for different values of M along with typical Fermi surfaces.

We separate the low and high SDW field M on two different panels to not overload the plot. For low enough values of M, the n_H curves deviate gradually from $M = 0$ (black). The Fermi surface is almost equivalent to the bare Fermi surface, with additional anticrossing at the antiferromagnetic zone boundary.

For high field ($M \geqslant 1$), the system reaches another regime where n_H is precisely proportional to p near half-filling. This regime corresponds to an antiferromagnetic field M so strong that it separates the original band into two new bands. Indeed, the curves are plotted as a function of the doping p, but if they were plotted as a function of the chemical potential, we would observe a gap at half-filling $p = 0$; there would be a range of chemical potential with $n_H = 0$. In fact, if we compare to the bare band behavior, we see that the pattern displayed in Fig. 2 is repeated twice: hence the equivalence to two separated bands.

From these results we can reproduce what was already published by Storey [3], simply by varying M as a function of p. This corresponds to picking points from different curves depending on the value of $M(p)$ in the model. If we zoom on the portion $p = 0$ to $p = 0.3$ and vary the field M linearly as a function of p, we also obtain that n_H goes from p to $1 + p$. It is, however, not realistic to consider an antiferromagnetic regime

for $p > 0.05$ in hole-doped cuprates [21]. For this reason, we consider SDWs that are incommensurate and collinear in the next section.

C. Incommensurate SDW ($\delta = 1/6$)

In Fig. 4, we show precisely the same quantities as in Fig. 3, but for incommensurate SDW with $\delta = 1/6$.

For $M < 1.0$, the behavior is similar to the antiferromagnetic case. For $M \geqslant 1.0$, the behavior is much more complicated but reaches a stable regime for $M \geqslant 4.0$. We then recognize something similar to the $M = 4.0$ curve of Fig. 3: the strong field M causes multiple band splittings. In fact, we have precisely $2L = 6$ bands when $\delta = 1/6$. Indeed, the original band (for $M = 0$) in the original Brillouin zone is split into six different portions, one for each rBz. Every rBz contains the same number of $\mathbf{k}$ points, hence the same number of states. In fact, n_H vanishes precisely when p is a multiple of $1/3$, in other words, $1/6$ of the total band electron. As M increases, these six bands separate completely from each other. The Hall number n_H thus presents signatures of these six independent bands. Note that if we chose $\delta = 1/8$ we would have eight different bands, and so on.

From this observation, we can conclude that, for the incommensurate case, the regime $M \gg t$ is unlikely to be the cause of the p behavior near half-filling, contrary to the commensurate case. Indeed, even if we find that $n_H \sim p$ in Fig. 4 around half-filling, the region over which we find this behavior decreases with $2L_y$. As the fractions δ considered are more and more incommensurate, in other words, as $2L_y$ increases, n_H is more and more constrained to zero when M is large. Thus we lose this $n_H \sim p$ behavior for incommensurate SDW at large M.

One could argue that, even if the $n_H \sim p$ behavior around half-filling is not obtained at high M, it could somehow appear at intermediate M, like the curve $M \sim 0.5$ of Fig. 4 seems to suggest. We study this case in the next section.

D. Constant M, different δ

Figure 5 shows how the parameter δ influences n_H. We choose $M = 1.0$ because it is not too large but still sufficient to find the $n_H \sim p$ behavior around half-filling for the commensurate antiferromagnetic case ($\delta = 0$) (see Fig. 3). In Fig. 5, we see that, for small δ, the result is close to the commensurate case. In other words, we find a behavior close to $n_H \sim p$ near half-filling. However, the more we increase δ, the more it deviates from $n_H \sim p$.

In the experiments, δ is a function of p [4,13,14]. Therefore, a natural question arises: is it possible to observe $n_H \sim p$ at low doping if we vary δ as a function of p?

E. Variable δ as a function of p

In Fig. 6, we look at the n_H curve when the experimentally observed $\delta(p)$ is used. We see that for these choices of δ as a function of p, n_H has a tendency to follow p, but is not locked to p. Note that we chose $\delta \sim p - 0.03$ as reported by experiments on YBCO [4], but choosing a slightly different δ dependency leads to the same conclusion. Also, as discussed before, increasing or decreasing M would make n_H deviate

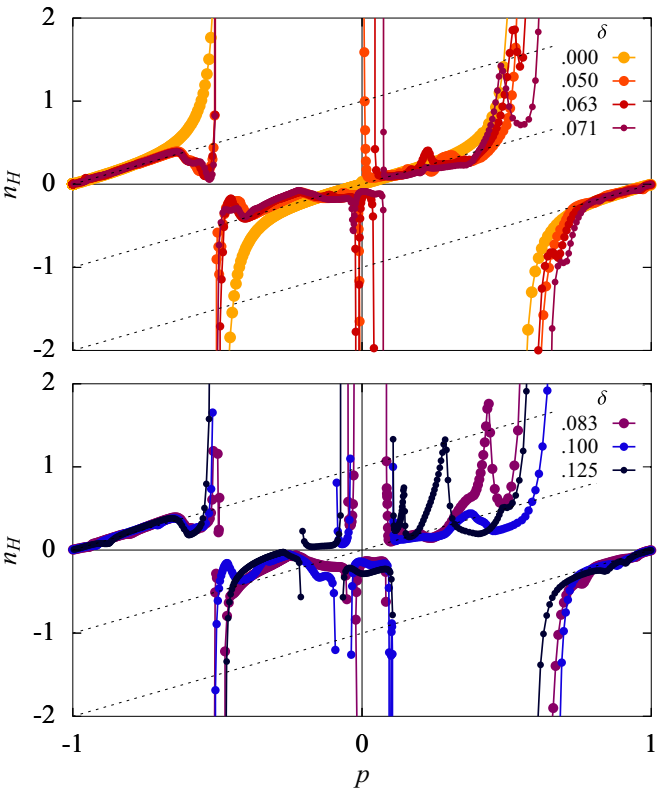

FIG. 5. Hall number n_H as a function of the hole doping p relative to half-filling for different SDW incommensurability δ with the same $M = 1.0$. We separate small and big δ on two panels to lighten the plot. The δ used are 0, $\frac{1}{20} = 0.050$, $\frac{1}{16} = 0.063$, $\frac{1}{14} = 0.071$, $\frac{1}{12} = 0.083$, $\frac{1}{10} = 0.100$, and $\frac{1}{8} = 0.125$. $t' = -0.3$ and $t'' = 0.2$.

even more from the p behavior around half-filling. We claim here that, for the model used, the parameters used in Fig. 6 are close to the best set of parameters to reproduce the $n_H \sim p$ behavior, yet it still lacks agreements with experiments [1,22,23].

On the same figure, we see that the Fermi surfaces corresponding to the best-case scenario are different from the ARPES results on YBCO [21,24]. In the experiments, if we ignore the effects of bilayer splitting and copper oxide chains, the Fermi surface only consists of four Fermi arcs. It is often speculated that those arcs are in fact four small pockets with their back spectral weight too faint to be measured. By contrast, in our computed Fermi surfaces, spectral weight remains in the y antinodes, and many copies of the nodal pocket appear along the y direction. These features are absent in experiments.

IV. DISCUSSION

Our analysis indicates that the incommensurate collinear SDW, as represented by our model, cannot explain the $n_H \sim p$ behavior of the underdoped YBCO measurements [1,22]. Even the best-case scenario ($M = 1$ and $\delta \sim p - 0.03$, as in Fig. 6) predicts important deviations from the $n_H \sim p$ behavior. Those deviations were not seen in experiments on YBCO [1,22]. However, Hall measurements in LSCO and BLSCO [18] report a sharp feature in n_H around $p = 0.16$, reminiscent of the deviation from $n_H \sim p$ we predict here, but

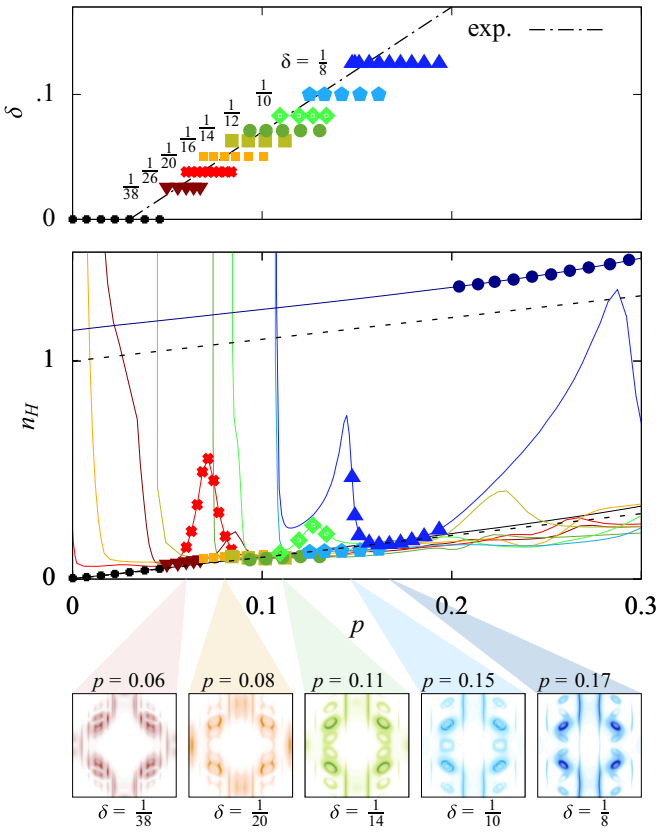

FIG. 6. The top panel shows the chosen distribution of δ values as function of p. Each symbol of a given color corresponds to the same incommensurability δ: 0, $\frac{1}{38} = 0.026$, $\frac{1}{26} = 0.038$, $\frac{1}{20} = 0.050$, $\frac{1}{16} = 0.063$, $\frac{1}{14} = 0.071$, $\frac{1}{12} = 0.083$, $\frac{1}{10} = 0.100$, and $\frac{1}{8} = 0.125$. The dotted line corresponds to the experimental reference $\delta \sim p - 0.03$ [4]. In the middle panel, Hall number n_H as a function of hole doping p relative to half-filling for different SDW incommensurability δ. We use $M = 1.0$ below $p = 0.2$ and $M = 0.0$ above. Each curve corresponds to a different δ. The symbols on the middle panel correspond to the symbols on the top panel. We only draw symbols on the portion of the curve that corresponds to the experimental reference $\delta \sim p - 0.03$. We also show the corresponding curve for the whole p range for each δ to highlight the deviations from $n_H \sim p$ close to the data points selected. In the bottom panels, we show Fermi surfaces for five different p and δ. The triangles above the Fermi surface graphs show the doping corresponding to each Fermi surface.

the authors argue this feature is linked to the high temperature superconducting mechanism. It could be worth investigating if this feature is not rather linked to density waves similar to those studied here.

Note also that we chose the values of M that provided the desired qualitative behavior of $n_H \sim p$. It does not imply any quantitative prediction. What we called the "best case scenario" (Fig. 6) is not a proof that M should have a value around 1, which is t in our units. In fact, the M corresponding to the real SDW found in YBCO should be much smaller than $M \sim 1$, since, for such large values of M, there are strong irregularities in the calculated Fermi surfaces, as shown in Fig. 6.

The results for the commensurate antiferromagnetic case shown in Fig. 3 can, however, explain the Hall effect measurements in electron-doped $Pr_{2x}Ce_xCuO_4$ [25] and $La_{2x}Ce_xCuO_4$ [26], where x, the doping in electrons, corresponds to $x = -p$ on the electron doped side. Indeed, starting from $p = 0$, if we decrease M as we decrease p (increase x), at some point there will be a sign change in n_H, as observed experimentally in Refs. [25,26]. This is one possible explanation of the p to $1 + p$ (or $-x$ to $1 - x$) transition in the electron-doped cuprates. Note, however, as argued in Refs. [25,26], that the proximity of the vHs to $p = 0$ remains a plausible alternative explanation.

We must stress that the conclusions reached here, with the incommensurate collinear SDW, do not extend to the incommensurate spiral SDW, as both orders are fairly different [they are only the same for $\mathbf{Q} = (\pi,\pi)$]. Indeed, this explains the significant difference between the results of our model and the results of Eberlein *et al.* [5]. The local moment in a spiral SDW is constant in magnitude but its direction rotates, whereas the local moment in a collinear SDW has a fixed direction but its amplitude is modulated. It is also possible to model a truly incommensurate $\mathbf{Q}$ spiral with a 2×2 matrix (two-band model), without any approximation [5]. The value of $\mathbf{Q}$ can be as incommensurate as needed. With the method presented in this article, a truly incommensurate collinear SDW would necessitate a matrix of infinite size.

A natural extension of this study would be to average over a spread in $\mathbf{Q}$ vector to simulate shorter range correlations. Indeed, in the large M limit, as shown in Fig. 4, there are precisely $2L + 1$ peaks (at values of p where $R_H = 0$), which is an artifact of commensurability in our approach. So, averaging over a spread in $\mathbf{Q}$ vector would smear out the fine details of the Fermi surface and possibly smear the peaks in n_H (Fig. 6), resulting in $n_H \sim p$ behavior. Adding disorder to the model would probably result in a similar effect. This is outside the scope of the model presented here, but it would be interesting to verify this point in future work. In any case, there are multiple refinements needed to reproduce the $n_H \sim p$ behavior with incommensurate collinear SDW, whereas two-band effective models [3,5,7,8] do not need any impurities, $\mathbf{Q}$ averaging, or fine-tuned value of the effective mean field M to obtain the $n_H \sim p$. From previous studies of these models [3,5,7,8], we know that two-band effective models are sufficient to obtain the $n_H \sim p$ behavior because they open a gap at half-filling. By contrast, the incommensurate SDW studied here splits the dispersion in more than two bands, which causes deviations from the seeked $n_H \sim p$ behavior. We can infer that the opening of a gap at half-filling might be an important necessary feature of any adequate theory of the zero-temperature normal state in the pseudogap regime. Nonetheless, the actual physics behind the pseudogap at zero temperature is probably more subtle, being deeply rooted in strongly correlated physics as indicated by methods like cluster perturbation theory [27,28] or generalizations of dynamical mean-field theory to clusters, like cellular dynamical mean-field theory CDMFT or the dynamical cluster approximation DCA [29–41]. It would be interesting to calculate the value of n_H for the pseudogap regime with these techniques in future work.

ACKNOWLEDGMENTS

We acknowledge S. Badoux, I. Garate, R. Nourafkan and L. Taillefer for discussions. This work was partially supported by the Canada First Research Excellence Fund, the Natural Sciences and Engineering Research Council (Canada) under Grant No. RGPIN-2014-04584 and the Research Chair on the Theory of Quantum Materials (A.-M.S.T.). Simulations were performed on computers provided by the Canadian Foundation for Innovation, the Ministere de l'Éducation des Loisirs et du Sport (Québec), Calcul Québec, and Compute Canada.

APPENDIX A: DERIVATIVES OF EIGENENERGIES

Expressions for the conductivities σ_{xx} and σ_{xy} contain the derivative of the eigenenergies of the Hamiltonians $\frac{\partial E_{\mathbf{k},n}}{\partial k_\alpha}$ and $\frac{\partial^2 E_{\mathbf{k},n}}{\partial k_\alpha \partial k_\beta}$. For a two-band model like the antiferromagnet, the calculation is straightforward. However, for larger matrices (size 3 or more), the analytic expression of the eigenvalues is much more complicated and one must rely on a numerical approach. We could find the derivatives with finite differences but there is imprecision around degeneracies due to the arbitrary ordering of the eigenenergies $E_{\mathbf{k},n}$ (for some specific $\mathbf{k}$ points). It is important to optimize this diagonalization since it is the bottleneck of the calculation for large L_y. In this appendix, we present a general and straightforward approach to calculate exactly these derivatives for any $\mathbf{k}$.

1. First derivative

The first derivative $\frac{\partial E_{\mathbf{k},n}}{\partial k_\alpha}$ is obtained from the Hellmann-Feynman theorem. Here we recall the proof. Starting from the eigenequation (ignoring the spin index here):

$$\hat{H}_{\mathbf{k}}|\psi_{\mathbf{k},n}\rangle = E_{\mathbf{k},n}|\psi_{\mathbf{k},n}\rangle, \tag{A1}$$

where $\mathbf{k}$ is the wave vector, $\hat{H}_{\mathbf{k}}$ is the Hamiltonian operator, and $E_{\mathbf{k},n}$ are the eigenenergies corresponding to the eigenstates $|\psi_{\mathbf{k},n}\rangle$. Let us drop the explicit $\mathbf{k}$ in the notation from here. The eigenbasis is orthonormal:

$$\langle\psi_n|\psi_m\rangle = \delta_{n,m} \tag{A2}$$

$$\frac{\partial}{\partial k_\alpha}\langle\psi_n|\psi_n\rangle = \frac{\partial\langle\psi_n|}{\partial k_\alpha}|\psi_n\rangle + \langle\psi_n|\frac{\partial|\psi_n\rangle}{\partial k_\alpha} = 0. \tag{A3}$$

Multiplying (A1) by $\langle\psi_n|$ and taking the derivative, we obtain

$$\frac{\partial}{\partial k_\alpha}\langle\psi_n|\hat{H}|\psi_n\rangle = \langle\psi_n|\frac{\partial\hat{H}}{\partial k_\alpha}|\psi_n\rangle + \underbrace{\frac{\partial\langle\psi_n|}{\partial k_\alpha}E_n|\psi_n\rangle + \langle\psi_n|E_n\frac{\partial|\psi_n\rangle}{\partial k_\alpha}}_{=0}. \tag{A4}$$

The last two terms vanish because of Eq. (A3). Using the eigenequation on the left-hand term, we find:

$$\frac{\partial E_n}{\partial k_\alpha} = \langle\psi_n|\frac{\partial\hat{H}}{\partial k_\alpha}|\psi_n\rangle, \tag{A5}$$

which is known as the Hellmann-Feynman theorem [16,17].

2. Second derivative

For the second derivative, the approach is similar. Taking the derivative of Eq. (A5), we obtain three terms:

$$\frac{\partial^2 E_n}{\partial k_\beta \partial k_\alpha} = \langle\psi_n|\frac{\partial^2\hat{H}}{\partial k_\beta \partial k_\alpha}|\psi_n\rangle + \frac{\partial\langle\psi_n|}{\partial k_\beta}\frac{\partial\hat{H}}{\partial k_\alpha}|\psi_n\rangle + \langle\psi_n|\frac{\partial\hat{H}}{\partial k_\alpha}\frac{\partial|\psi_n\rangle}{\partial k_\beta}. \tag{A6}$$

The first term is straightforward to calculate but the last two terms must be further simplified. The derivative with respect to k_α of the eigenequation (A1) can be reordered as

$$\frac{\partial\hat{H}}{\partial k_\alpha}|\psi_n\rangle = \frac{\partial E_n}{\partial k_\alpha}|\psi_n\rangle - (\hat{H} - E_n)\frac{\partial|\psi_n\rangle}{\partial k_\alpha}, \tag{A7}$$

which can be substituted twice in Eq. (A6). We obtain multiple terms, two of which cancel due to Eq. (A3):

$$\frac{\partial^2 E_n}{\partial k_\beta \partial k_\alpha} = \langle\psi_n|\frac{\partial^2\hat{H}}{\partial k_\beta \partial k_\alpha}|\psi_n\rangle - 2\frac{\partial\langle\psi_n|}{\partial k_\beta}(\hat{H} - E_n)\frac{\partial|\psi_n\rangle}{\partial k_\alpha}. \tag{A8}$$

Note that we could not isolate $\frac{\partial|\psi_n\rangle}{\partial k_\alpha}$ directly in Eq. (A7) because, by definition of the eigenvalues E_n, the determinant of $(\hat{H} - E_n)$ is zero, thus $(\hat{H} - E_n)$ cannot be inverted.

Form Eq. (A8) is simpler, but we still need to determine correctly the derivative of the eigenstate $\frac{\partial|\psi_n\rangle}{\partial k_\alpha}$. This can be calculated exactly using perturbation theory. Starting with the definition of the derivative (in one dimension k for simplicity):

$$\frac{\partial|\psi_n(k)\rangle}{\partial k} = \lim_{\delta k\to 0}\frac{|\psi_n(k+\delta k)\rangle - |\psi_n(k)\rangle}{\delta k}. \tag{A9}$$

The Hamiltonian $\hat{H}(k+\delta k)$ has $|\psi_n(k+\delta k)\rangle$ as eigenstates. Since δk is small by definition and the eigenenergies vary smoothly as a function of k, the Hamiltonian at $k+\delta k$ can be expressed by a small perturbation from $\hat{H}(k)$:

$$\hat{H}(k+\delta k) = \hat{H}(k) + \underbrace{[\hat{H}(k+\delta k) - \hat{H}(k)]}_{\text{perturbation}}. \tag{A10}$$

Since $\delta k \to 0$ in Eq. (A9), the first order perturbation term of $|\psi_n(k+\delta k)\rangle$ is exact:

$$|\psi_n(k+\delta k)\rangle - |\psi_n(k)\rangle = \sum_{m\neq n}\frac{\langle\psi_m(k)|(\hat{H}(k+\delta k) - \hat{H}(k))|\psi_n(k)\rangle}{E_n(k) - E_m(k)}|\psi_m(k)\rangle. \tag{A11}$$

Substituting Eq. (A11) into Eq. (A9), we obtain

$$\frac{\partial|\psi_n\rangle}{\partial k_\alpha} = \sum_{m\neq n}\frac{\langle\psi_m|\frac{\partial\hat{H}}{\partial k_\alpha}|\psi_n\rangle}{E_n - E_m}|\psi_m\rangle, \tag{A12}$$

which holds for any dimension of k space. This formula is commonly used in the calculation of the Berry connection [42,43].

Substituting in Eq. (A8), we find the band version of the f-sum rule [44,45]

$$\frac{\partial^2 E_n}{\partial k_\beta \partial k_\alpha} = \langle\psi_n|\frac{\partial^2 \hat{H}}{\partial k_\beta \partial k_\alpha}|\psi_n\rangle + 2\sum_{m\neq n}\frac{\langle\psi_n|\frac{\partial \hat{H}}{\partial k_\beta}|\psi_m\rangle\langle\psi_m|\frac{\partial \hat{H}}{\partial k_\alpha}|\psi_n\rangle}{E_n - E_m}. \quad \text{(A13)}$$

Since the derivatives of the Hamiltonian matrix are easy to obtain analytically, the only numerical part of the calculation that must be performed at any **k** point is the diagonalization of the Hamiltonian to obtain the eigenvalues.

APPENDIX B: VAN HOVE SINGULARITY ENERGY

Here, we derive a simple equation to find the energy corresponding to the van Hove singularity in a tight-binding model with the dispersion in Eq. (2).

The van Hove singularities occur at $\frac{\partial \xi_{\mathbf{k}}}{\partial k_x} = \frac{\partial \xi_{\mathbf{k}}}{\partial k_y} = 0$, where

$$\frac{\partial \xi_{\mathbf{k}}}{\partial k_x} = 2t\sin(k_x) + 4t''\sin(2k_x) + 2t'(\sin(k_x + k_y) + \sin(k_x - k_y)) \quad \text{(B1)}$$

and similar for $\frac{\partial \xi_{\mathbf{k}}}{\partial k_y}$. If we focus on the singularities that can be found on the axis $k_y = 0$, we obtain k_x where the saddle point in the energy is

$$\tilde{k}_x = \begin{cases} \arccos(r) & \text{if } |r| \leqslant 1 \\ \pi & \text{otherwise} \end{cases}, \quad \text{(B2)}$$

$$\text{where} \quad r \equiv -\frac{t + t'}{4t''}. \quad \text{(B3)}$$

Using some trigonometric identities in Eq. (2) together with Eq. (B2), we can calculate that the energy corresponding to this saddle point is

$$\xi_{\mathbf{k}=(\tilde{k}_x,0)} = \begin{cases} -2t(1+r) - 4t'r - 4t''r^2 & \text{if } |r| \leqslant 1 \\ -4t' - 4t'' & \text{otherwise} \end{cases}. \quad \text{(B4)}$$

This reduces to the result of Ref. [46] when $t'' = 0$. Note that, to be general, we would need to search for singularities that cannot be found on the axis $k_x = 0$ or $k_y = 0$, but when t' and t'' are small compared to t, as in every cuprate material, the saddle points can only be found on the axis $k_x = 0$ or $k_y = 0$. This can be seen on the Fermi surfaces of Fig. 2: the van Hove singularities are only found on the axis $k_x = 0$ and $k_y = 0$.

[1] S. Badoux, W. Tabis, F. Laliberté, G. Grissonnanche, B. Vignolle, D. Vignolles, J. Béard, D. A. Bonn, W. N. Hardy, R. Liang, N. Doiron-Leyraud, L. Taillefer, and C. Proust, Nature **531**, 210 (2016).

[2] J. L. Tallon and J. W. Loram, Physica C **349**, 53 (2001).

[3] J. G. Storey, EPL (Europhys. Lett.) **113**, 27003 (2016).

[4] D. Haug, V. Hinkov, Y. Sidis, P. Bourges, N. B. Christensen, A. Ivanov, T. Keller, C. T. Lin, and B. Keimer, New J. Phys. **12**, 105006 (2010).

[5] A. Eberlein, W. Metzner, S. Sachdev, and H. Yamase, Phys. Rev. Lett. **117**, 187001 (2016).

[6] K.-Y. Yang, T. M. Rice, and F.-C. Zhang, Phys. Rev. B **73**, 174501 (2006).

[7] S. Chatterjee and S. Sachdev, Phys. Rev. B **94**, 205117 (2016).

[8] S. Verret, O. Simard, M. Charlebois, D. Sénéchal, and A.-M. S. Tremblay, Phys. Rev. B **96**, 125139 (2017).

[9] C. Morice, X. Montiel, and C. Pépin, Phys. Rev. B **96**, 134511 (2017).

[10] N. B. Christensen, H. M. Rønnow, J. Mesot, R. A. Ewings, N. Momono, M. Oda, M. Ido, M. Enderle, D. F. McMorrow, and A. T. Boothroyd, Phys. Rev. Lett. **98**, 197003 (2007).

[11] J. C. Tung and G. Y. Guo, Phys. Rev. B **83**, 144403 (2011).

[12] Y. Tsunoda, J. Phys.: Condens. Matter **1**, 10427 (1989).

[13] K. Yamada, C. H. Lee, K. Kurahashi, J. Wada, S. Wakimoto, S. Ueki, H. Kimura, Y. Endoh, S. Hosoya, G. Shirane, R. J. Birgeneau, M. Greven, M. A. Kastner, and Y. J. Kim, Phys. Rev. B **57**, 6165 (1998).

[14] M. Fujita, K. Yamada, H. Hiraka, P. M. Gehring, S. H. Lee, S. Wakimoto, and G. Shirane, Phys. Rev. B **65**, 064505 (2002).

[15] P. Voruganti, A. Golubentsev, and S. John, Phys. Rev. B **45**, 13945 (1992).

[16] R. P. Feynman, Phys. Rev. **56**, 340 (1939).

[17] B. M. Deb, Chem. Phys. Lett. **17**, 78 (1972).

[18] F. F. Balakirev, J. B. Betts, A. Migliori, I. Tsukada, Y. Ando, and G. S. Boebinger, Phys. Rev. Lett. **102**, 017004 (2009).

[19] E. Pavarini, I. Dasgupta, T. Saha-Dasgupta, O. Jepsen, and O. K. Andersen, Phys. Rev. Lett. **87**, 047003 (2001).

[20] A. I. Liechtenstein, O. Gunnarsson, O. K. Andersen, and R. M. Martin, Phys. Rev. B **54**, 12505 (1996).

[21] M. A. Hossain, J. D. F. Mottershead, D. Fournier, A. Bostwick, J. L. McChesney, E. Rotenberg, R. Liang, W. N. Hardy, G. A. Sawatzky, I. S. Elfimov, D. A. Bonn, and A. Damascelli, Nat. Phys. **4**, 527 (2008).

[22] K. Segawa and Y. Ando, Phys. Rev. B **69**, 104521 (2004).

[23] Y. Ando, Y. Kurita, S. Komiya, S. Ono, and K. Segawa, Phys. Rev. Lett. **92**, 197001 (2004).

[24] J. Meng, G. Liu, W. Zhang, L. Zhao, H. Liu, X. Jia, D. Mu, S. Liu, X. Dong, J. Zhang, W. Lu, G. Wang, Y. Zhou, Y. Zhu, X. Wang, Z. Xu, C. Chen, and X. J. Zhou, Nature **462**, 335 (2009).

[25] Y. Dagan and R. L. Greene, arXiv:1612.01703.

[26] T. Sarkar, P. R. Mandal, J. S. Higgins, Y. Zhao, H. Yu, K. Jin, and R. L. Greene, arXiv:1706.07836.

[27] D. Sénéchal, D. Perez, and D. Plouffe, Phys. Rev. B **66**, 075129 (2002).

[28] D. Sénéchal and A.-M. S. Tremblay, Phys. Rev. Lett. **92**, 126401 (2004).

[29] G. Kotliar, S. Y. Savrasov, G. Pálsson, and G. Biroli, Phys. Rev. Lett. **87**, 186401 (2001).

[30] A. I. Lichtenstein and M. I. Katsnelson, Phys. Rev. B **62**, R9283 (2000).

[31] M. Civelli, M. Capone, S. S. Kancharla, O. Parcollet, and G. Kotliar, Phys. Rev. Lett. **95**, 106402 (2005).

[32] B. Kyung, S. S. Kancharla, D. Sénéchal, A.-M. S. Tremblay, M. Civelli, and G. Kotliar, Phys. Rev. B **73**, 165114 (2006).

[33] T. D. Stanescu and G. Kotliar, Phys. Rev. B **74**, 125110 (2006).
[34] A. Macridin, M. Jarrell, T. Maier, P. R. C. Kent, and E. D'Azevedo, Phys. Rev. Lett. **97**, 036401 (2006).
[35] K. Haule and G. Kotliar, Phys. Rev. B **76**, 104509 (2007).
[36] S. S. Kancharla, B. Kyung, D. Sénéchal, M. Civelli, M. Capone, G. Kotliar, and A.-M. S. Tremblay, Phys. Rev. B **77**, 184516 (2008).
[37] M. Ferrero, P. S. Cornaglia, L. De Leo, O. Parcollet, G. Kotliar, and A. Georges, Phys. Rev. B **80**, 064501 (2009).
[38] M. Ferrero, P. S. Cornaglia, L. D. Leo, O. Parcollet, G. Kotliar, and A. Georges, Europhys. Lett. **85**, 57009 (2009).
[39] S. Sakai, Y. Motome, and M. Imada, Phys. Rev. Lett. **102**, 056404 (2009).
[40] E. Gull, M. Ferrero, O. Parcollet, A. Georges, and A. J. Millis, Phys. Rev. B **82**, 155101 (2010).
[41] G. Sordi, K. Haule, and A.-M. S. Tremblay, Phys. Rev. B **84**, 075161 (2011).
[42] D. Xiao, M.-C. Chang, and Q. Niu, Rev. Mod. Phys. **82**, 1959 (2010).
[43] M. V. Berry, Proc. R. Soc. Lond. A **392**, 45 (1984).
[44] A. H. Wilson, Proc. Cambridge Philos. Soc. **49**, 292 (1953).
[45] H. Fukuyama, Prog. Theor. Phys. **45**, 704 (1971).
[46] P. Bénard, L. Chen, and A.-M. S. Tremblay, Phys. Rev. B **47**, 15217 (1993).